

# Monte Carlo Simulations of Water Pollutant Adsorption at Parts-per-Billion Concentration: A Study on 1,4-Dioxane

Samiha Sharlin, Rodrigo A. Lozano, and Tyler R. Josephson\*



Cite This: *J. Chem. Theory Comput.* 2024, 20, 5854–5865



Read Online

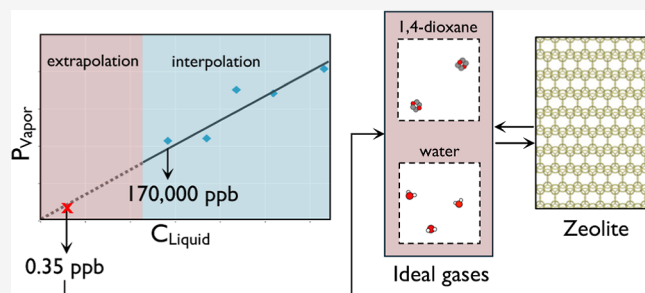
ACCESS |

Metrics & More

Article Recommendations

Supporting Information

**ABSTRACT:** 1,4-dioxane, an emerging water pollutant with high production volumes, is a probable human carcinogen. The inadequacy of conventional treatment processes demonstrates the need for an effective remediation strategy. Crystalline nanoporous materials are cost-effective adsorbents due to their high capacity and selective separation in mixtures. This study explores the potential of all-silica zeolites for the separation of 1,4-dioxane from water. These zeolites are highly hydrophobic and can preferentially adsorb nonpolar molecules from mixtures. We investigated six zeolite frameworks (BEA, EUO, FER, IFR, MFI, and MOR) using Monte Carlo simulations in the Gibbs ensemble. The simulations indicate high selectivity by FER and EUO, especially at low pressures, which we attribute to pore sizes and shapes with a greater affinity to 1,4-dioxane. We also demonstrate a Monte Carlo simulation workflow using gauge cells to model the adsorption of an aqueous solution of 1,4-dioxane at a 0.35 ppb concentration. We quantify 1,4-dioxane and water coadsorption and observe selectivities ranging from  $1.1 \times 10^5$  in MOR to  $8.7 \times 10^6$  in FER. We also demonstrate that 1,4-dioxane is in the infinite dilution regime in the aqueous phase at this concentration. This simulation technique can be extended to model other emerging water contaminants such as perfluoroalkyl and polyfluoroalkyl substances (PFAS), chlorofluorocarbons, and others, which are also found in extremely low concentrations.



## INTRODUCTION

Crystalline porous materials like metal–organic frameworks, covalent organic frameworks, carbon nanotubes, polyoxometalates, and zeolites have revolutionized mixture adsorption separations through control of pore size,<sup>1</sup> entropy,<sup>2</sup> and binding strength.<sup>3</sup> Additionally, their stability, tunability, and low cost make them versatile<sup>4</sup> – for example, zeolites are used as catalysts,<sup>5</sup> adsorbents,<sup>6</sup> and ion exchangers<sup>7</sup> in many chemical processes and have an increasingly rising global market of multibillion US dollars.<sup>8</sup> Water and wastewater remediation methods also extensively use zeolites for purification from ammonia,<sup>9</sup> heavy metals,<sup>10</sup> radioactive,<sup>11</sup> toxic,<sup>12</sup> and organic substances,<sup>13</sup> as well as for water softening<sup>14</sup> and seawater desalination.<sup>15</sup>

The basic building block of zeolites is a  $\text{TO}_4$  tetrahedron, where the T atom is usually silicon (Si) or aluminum (Al), forming an open crystal structure with a narrow distribution of molecule-sized pores. The tetrahedrons can form different (6-, 8-, or 12 rings) units that give different topologies with the same chemical composition.<sup>16</sup> Over 40 naturally occurring zeolite frameworks and 265 synthetic ones are recognized by the International Zeolite Association (IZA) Structure Commission as of early 2024.<sup>17</sup> Zeolites with a high silicon content (approaching an infinite Si/Al ratio) can be synthesized<sup>18,19</sup> because this class of zeolites does not have acid sites or polar

cations, they can be highly hydrophobic and are exceptionally efficient as adsorbents in aqueous separations.<sup>13,20</sup>

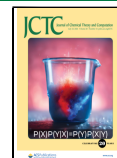
This study investigates the adsorption of 1,4-dioxane from water using all-silica zeolites at environmental concentrations using molecular simulations. 1,4-dioxane is an emerging contaminant and a probable human carcinogen<sup>21</sup> that has received less regulatory attention than other pollutants despite being frequently detected in high exceedance rates according to the third unregulated contaminant monitoring rule.<sup>22</sup> It is a stable cyclic diether with symmetrical ether connections. A negative octanol–water partitioning coefficient and a low carbon partitioning coefficient make leaching into the water from soil natural.<sup>23</sup> Recent studies show that over 30 million Americans consume water exceeding the health-based recommended threshold of 0.35 ppb.<sup>24</sup> To comply with the standards, several remediation strategies, including chemical, physical, and biological processes, are being evaluated; however, a practical solution for large-scale treatment is still in the works.<sup>25</sup> While

Received: February 23, 2024

Revised: June 11, 2024

Accepted: June 12, 2024

Published: July 10, 2024



enhanced oxidation and bioremediation techniques have potential, they are costly and complicated to execute in practical settings.<sup>25</sup> As degradation technologies are still developing, considerable mitigation efforts may well focus on treating surface and groundwater bodies to comply with the increasingly stringent limits to drinking water supplies. While these methods might fail to degrade water pollutants entirely, they can act as an interim that can potentially concentrate contaminants for subsequent remedial actions.

Common adsorbents like synthetic resins<sup>26</sup> and activated carbon<sup>27</sup> have not been cost-effective solutions for large-scale treatment of 1,4-dioxane due to their limited adsorptive capacity. Meanwhile, in one study, titanium silicalite-1, a zeolite, has shown higher capacity and faster adsorption kinetics due to its hydrophobicity.<sup>28</sup> Hydrophobic all-silica zeolites with comparable pore sizes may help address this challenge, but more insight is needed to determine its efficacy. For our investigation, we selected six frameworks (BEA, EUO, FER, IFR, MFI, and MOR) from the IZA database<sup>17</sup> based on their commercial availability,<sup>29</sup> crystallographic R-factor in high silica form,<sup>30</sup> and pore sizes comparable to 1,4-dioxane.<sup>28</sup> The pore landscapes of the zeolites are shown in Figure S1 and Table S1 summarizes their unit cell parameters.

The optimal design of an adsorbent is a challenging task and requires a broad understanding of the sorption process at the microscopic level. Molecular simulations provide invaluable access to thermodynamic phenomena occurring at the pore sites and thus have significantly contributed to the synthesis and applications of zeolite.<sup>16,31,32</sup> Additionally, adsorption systems with competition between complex adsorbates onto complex adsorbents can be better understood and more clearly evaluated through computer simulations.<sup>33,34</sup> For example, molecular dynamics has been used to study 1,4-dioxane transport and adsorption into Ti-silicalite in the presence of organic contaminants.<sup>28</sup>

However, the traditional simulation approach for modeling such a system is not only impractical but also impossible since the concentrations of 1,4-dioxane in the environment are typically in parts-per-billion ranges.<sup>24</sup> After all, a liquid simulation box with 1 solute molecule at 1 ppb concentration will have on the order of 1 billion water molecules.

This work introduces a simulation workflow for thermodynamic extrapolation using the gauge cell Monte Carlo (gcMC) technique to efficiently model the liquid phase adsorption of extremely low-concentration species from mixtures. The gcMC method enables control of density for each system component individually and has successfully modeled thermodynamically metastable and unstable systems that are typically inaccessible.<sup>35–38</sup> The method has been successfully implemented to investigate the phase behavior of fluids in confined spaces, including capillary condensation,<sup>39</sup> droplet formation,<sup>37,40</sup> and surfactant separation.<sup>41</sup>

Other methods of thermodynamic extrapolation include temperature extrapolation of Henry's Law constants<sup>42</sup> and extrapolating free energy landscapes;<sup>43</sup> however, we need to extrapolate in *concentration*, and these methods may be inaccurate if state points deviate significantly from reference points. A related work by Cichowski et al.<sup>44</sup> uses an expanded ensemble MC method with a transition matrix to estimate Henry's Law constant at infinite dilution, which aligns more closely with our research goals. In another study by Luo and Farrel,<sup>45</sup> the adsorption of trichloroethylene (TCE) from water was examined using Grand Canonical MC (GCMC)

simulations. They sampled TCE in an aqueous solution at concentrations equivalent to 1% of its saturation concentration. Our study extends to sampling water contaminants at parts-per-billion levels, which is typical of environmental conditions. While we apply this approach using Gibbs ensemble simulations, we note that it should also be compatible with simulations in the GC ensemble with a few modifications. The thermodynamic reservoir fixing the chemical potential will replace the gauge cells, and extrapolation will be performed by adjusting the chemical potential of the solute accordingly after establishing the relationship between  $\mu$  and concentration in infinite dilution conditions. Performing GCMC simulations at the pressure of interest for the liquid mixtures will require iterative adjustment of simulation settings until the target pressure is reached, as GCMC fixes  $\mu VT$  and measures  $p$ , unlike our approach, which fixes  $NpT$  and measures  $\mu$ .

We performed MC simulations in the MC for Complex Chemical Systems-Minnesota (MCCCS-MN) software<sup>46</sup> using classical force fields. First, we reproduced the vapor–liquid equilibrium properties of 1,4-dioxane for validation and then simulated the vapor and liquid phase adsorptions of 1,4-dioxane into the selected zeolite frameworks. The pure adsorption isotherms provided insight into the effects of pore size and shape on loading capacities. Finally, we investigated the selectivity of 1,4-dioxane for mixture adsorption from water at the health-based reference concentration (0.35 ppb), exploiting the gauge cell method, and constructing supercells for the zeolite frameworks.

## METHODS

**Thermodynamic Extrapolation Approach.** The gcMC method employs multiple simulation boxes, with one simulation box for the system of interest in chemical equilibrium with gauge cells for each component. The addition or removal of particles from the gauge cell instantly changes its chemical potential, and it is this variation that enables us to measure the chemical potential of the species for the system of interest and under the conditions of our interest. The approach was initially developed to construct the full-phase diagram of a confined fluid in the form of a van der Waals loop, which includes stable, metastable, and unstable equilibrium states.<sup>35</sup> In this work, the liquid simulation box is modeled as flexible with intermolecular interactions containing a dilute solution of 1,4-dioxane, while the gauge cells for each component are modeled as rigid and treated as ideal gas boxes. Simulations were set up in the isobaric–isothermal Gibbs ensemble ( $NpT$ -Gibbs),<sup>47–49</sup> where interbox swaps were performed for the particles between the simulation box representing the system of interest and gauge cell of each respective component. Volume moves were performed only on the simulation box representing the mixture solution. The Gibbs free energy of transfer,  $\Delta G_{14DX}^{*0}$ <sup>50,51</sup> for 1,4-dioxane, can then be computed from the ratio of densities in the simulation boxes

$$\Delta G_{14DX}^{*0} = kT \left[ \ln \left( \frac{\rho_{14DX}^{GC}}{\rho_{14DX}^{mix}} \right)_{eq} \right] \quad (1)$$

where  $k$ ,  $T$ ,  $\rho_{14DX}^{GC}$  and  $\rho_{14DX}^{mix}$  are the Boltzmann constant, temperature, and number densities of 1,4-dioxane in the gauge cell and mixture cell, respectively. A detailed derivation of eq 1 can be found in Supporting Information. We used eq 1 to determine the free energy of transfer for the dilute system of 1,4-

## Thermodynamic extrapolation approach

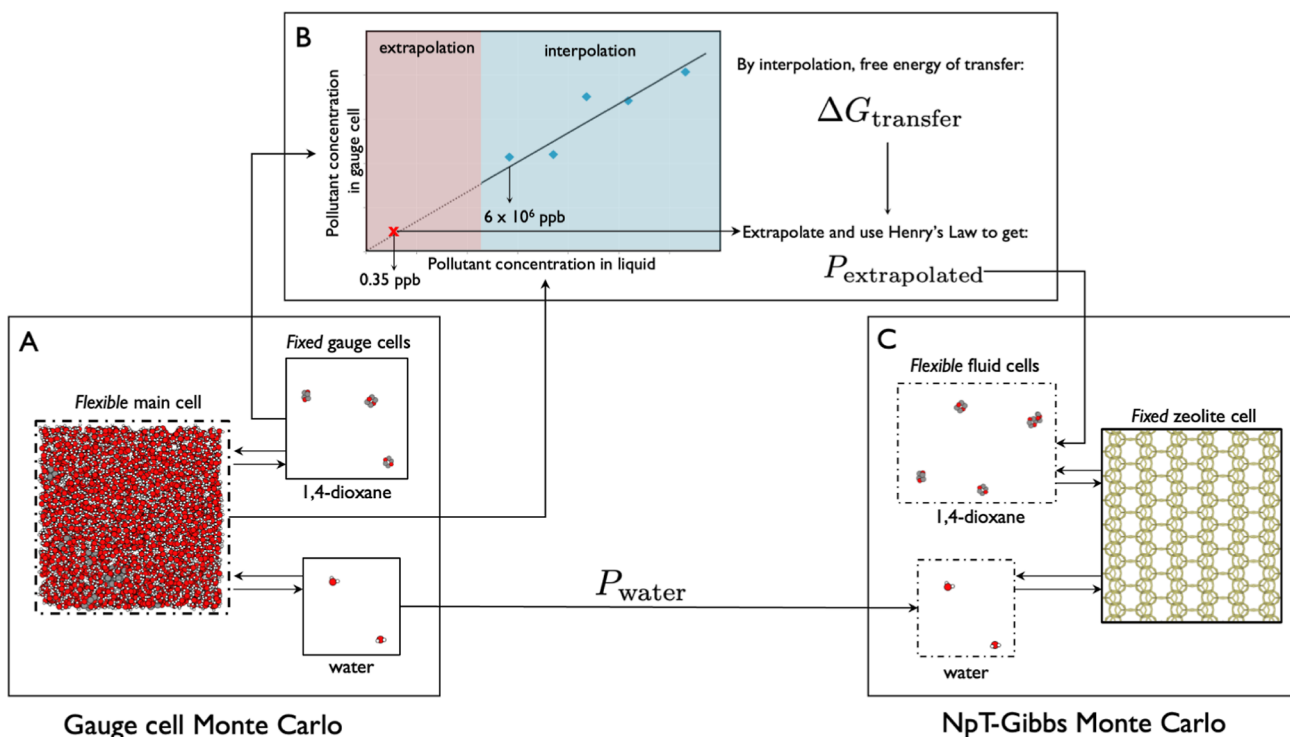


**Figure 1.** Thermodynamic extrapolation approach for dilute simulations. The first step (A) involves gcMC simulations with a dilute solution of 1,4-dioxane and water in the liquid simulation box, in chemical equilibrium, with two fixed ideal gas gauge cells that measure the partial pressures of 1,4-dioxane and water. We adjust the size of the 1,4-dioxane gauge cell to sample low concentrations in the liquid simulation box. The second step (B) involves obtaining the free energy of transfer from low-concentration state points, demonstrating the solute is in the Henry's law regime, and then assuming that  $\Delta G_{\text{transfer}}$  extrapolates to 0.35 ppb concentration. The 1,4-dioxane concentration in the gauge cell is calculated from eq 1, and the ideal gas law provides the extrapolated partial pressure. In the final step (C), NpT-Gibbs ensemble simulations use the extrapolated pressure for 1,4-dioxane while keeping the water pressure constant, thus imposing the equivalent chemical potentials of the dilute mixture onto a zeolite box.

dioxane. For extrapolation, we took the average  $\Delta G_{14DX}^{*0}$  of low-concentration state points and computed the 1,4-dioxane concentration in the gauge cell that would correspond to 0.35 ppb<sup>24</sup> in the environment. Since the concentration range is exceptionally low, we used Henry's Law to compute the corresponding partial pressure. Then, we set up NpT-Gibbs ensemble simulations with zeolite frameworks to model adsorption from low-concentrated liquid mixtures. In Figure 1, we briefly outline our method for the capture of 1,4-dioxane from water.

**Model and Algorithmic Details.** Transferable potentials for phase equilibria (TraPPE)<sup>52</sup> force fields were used to model 1,4-dioxane with TraPPE-UA,<sup>53</sup> and the zeolites were modeled using TraPPE-zeo.<sup>54</sup> Lennard-Jones (LJ) potentials were used for short-range van der Waals interactions, and Coulomb potentials were used for long-range electrostatic interactions with a spherical cutoff of 14 Å. Beyond this cutoff, analytical tail corrections were applied for LJ and Ewald summations for Coulomb interactions. However, the vapor box was less dense for lower temperature state points, and thus, a larger cutoff (approximately 30% of box length) was used to accommodate 10–20% of the molecules in the system. As Ewald convergence parameters are set automatically based on rcut and simulation box length, modifying rcut is common in low-temperature VLE simulations in the Gibbs ensemble.<sup>55</sup>

As with the standard TraPPE force fields, here the bond lengths were treated as fixed, bend angles with the simple

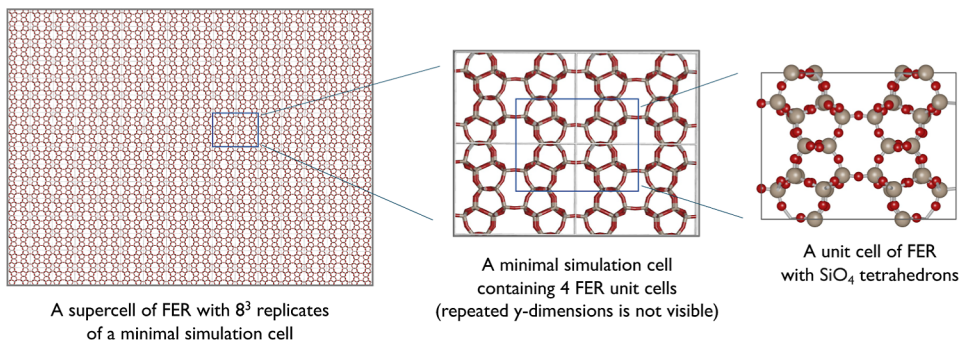
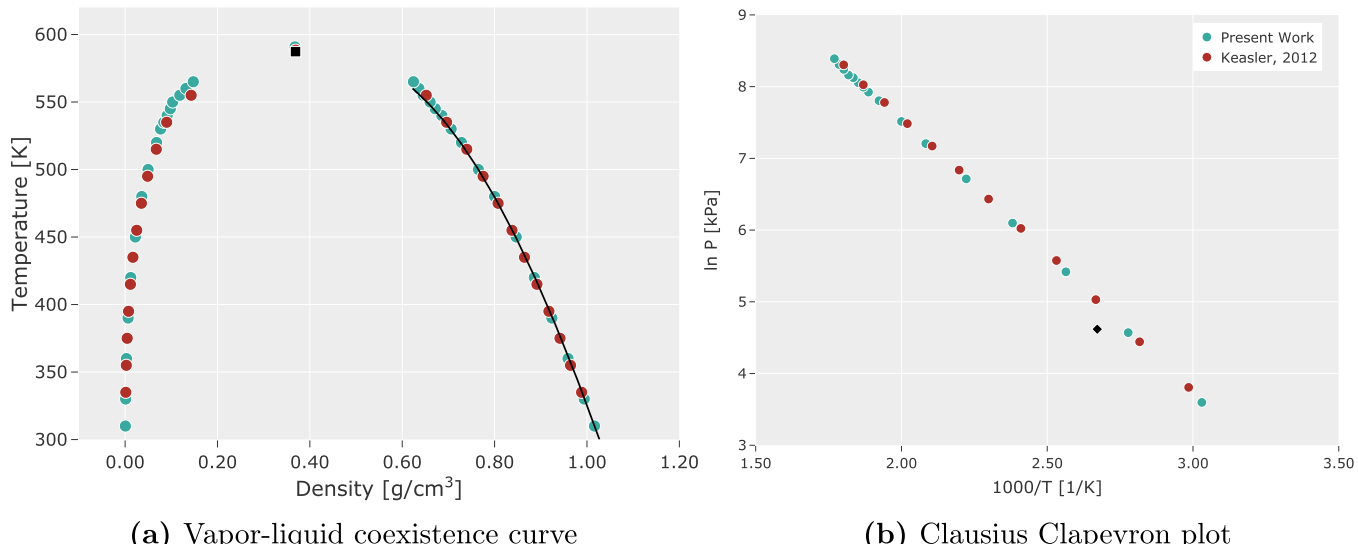
harmonic oscillator, and dihedrals with a cosine series (eq 2) of the form

$$\begin{aligned} u_{\text{torsion}}(\phi) = & c_0 + c_1[1 + \cos(\phi)] + c_2[1 - \cos(2\phi)] \\ & + c_3[1 + \cos(3\phi)] \end{aligned} \quad (2)$$

where  $\phi$  is the dihedral angle and  $c$  is constant.

The TraPPE-zeo model considers zeolites as a rigid framework with silicon and oxygen atoms fixed on their original crystallographic positions. Their interaction potentials are tabulated as grid points, which can be interpolated to give energy, depending on the location of adsorbent species in the simulation boxes. Additionally, the TIP4P model was used for water<sup>56</sup> in the mixture adsorption systems, as it has been shown to work well with the TraPPE force field for organic molecules.<sup>54,57–61</sup> All the model parameters used for this study are summarized in Table S2 of Supporting Information. The adsorption simulations were initialized with an empty zeolite box to prevent overlap issues for both unary and mixture systems.

Simulations were performed in the NVT-Gibbs ensemble for modeling the vapor–liquid equilibrium properties, and NpT-Gibbs was used for both adsorption and gauge cell systems.<sup>47–49</sup> MC simulations generate a sequence of states as a Markov chain with sampling probabilities corresponding to the ensemble's configurational integral.<sup>62,63</sup> Intramolecular and intermolecular energies are sampled efficiently using strategic MC moves, which are constrained by their alignment with the chosen

**Figure 2.** Scheme of supercell construction.**Figure 3.** Vapor–liquid coexistence curves and Clausius–Clapeyron plot for 1,4-dioxane. Experimental critical temperature ( $\blacksquare T_c$ ) and data, including normal boiling temperature ( $\blacklozenge T_b$ ), are shown in black symbols and solid lines. Simulation uncertainties are smaller than symbol size.

ensemble and their adherence to the detailed balance defined by the Metropolis acceptance criteria.<sup>64</sup>

The Gibbs ensemble consists of two (or more) simulation boxes with a constant total number of molecules without explicit interfaces. In such a system, the interbox swap move is integral to balancing the chemical potentials in addition to the regular translation, rotation, and volume moves. Configurational-bias MC (CBMC)<sup>65–67</sup> moves were also employed to sample configurations within each simulation box, as well as interbox swap moves. In regular CBMC, a molecule is grown bead by bead, with  $k$  trial positions generated based on the internal energy for each bead, and the external energy is computed for each trial position  $j$  of each bead  $i$ . One of these trial positions is selected and added to the existing chain, with a probability of

$$P_i(j) = \frac{e^{-\beta U_i^{\text{ext}}(j)}}{\sum_{l=1}^k e^{-\beta U_i^{\text{ext}}(l)}} \quad (3)$$

and  $\beta = 1/k_B T$ , where  $k_B$  is the Boltzmann constant and  $T$  is the temperature.<sup>68</sup>

The process was repeated until the entire molecule was grown. Various approaches to CBMC exist in the literature,<sup>66,67,69–72</sup> each with a different method of bead growth tailored to specific conformations of molecules. 1,4-dioxane, for instance, is challenging to grow with regular CBMC because the ring structure constrains its conformational space. The growth of such cyclic molecules requires an additional bias to nudge the

growth toward positions that will result in ring closures; here, we use the self-adapting fixed-end point CBMC developed by Wick and Siepmann.<sup>73</sup> The bias was introduced through guiding probabilities obtained from a short presimulation with only translational and rotational degrees of freedom. The probabilities are normalized ensemble-averaged bead–bead distance distributions that adapt during the simulation of the system of interest. Thus, the swap moves for 1,4-dioxane were performed, holding the ring conformation rigid while allowing multiple trial orientations to be explored.

**Supercell Construction.** Our cutoff radius in the zeolite box is 14 Å, so each zeolite box must be at least 28 Å in each dimension. Since zeolite unit cells are typically smaller than this, we used the smallest integer multiple in each dimension to construct the minimal simulation cell. For example, the FER (type 2) framework requires 2 unit cells in the  $x$ -direction, 4 in  $y$ , and 2 in  $z$ . Then, we constructed larger supercells by multiplying all dimensions by factors of 2, 4, and 8. **Figure 2** shows the scheme of the supercell construction for the FER framework. For simplicity, we only show a single unit cell of FER, its minimal simulation cell, and the largest supercell (minimal simulation cell  $\times$  512) used as the zeolite simulation box in mixture adsorption systems. As the interactions within the zeolite frameworks are pretabulated,<sup>74</sup> we can easily increase the zeolite simulation box size to model the supercells without incurring additional computational costs.

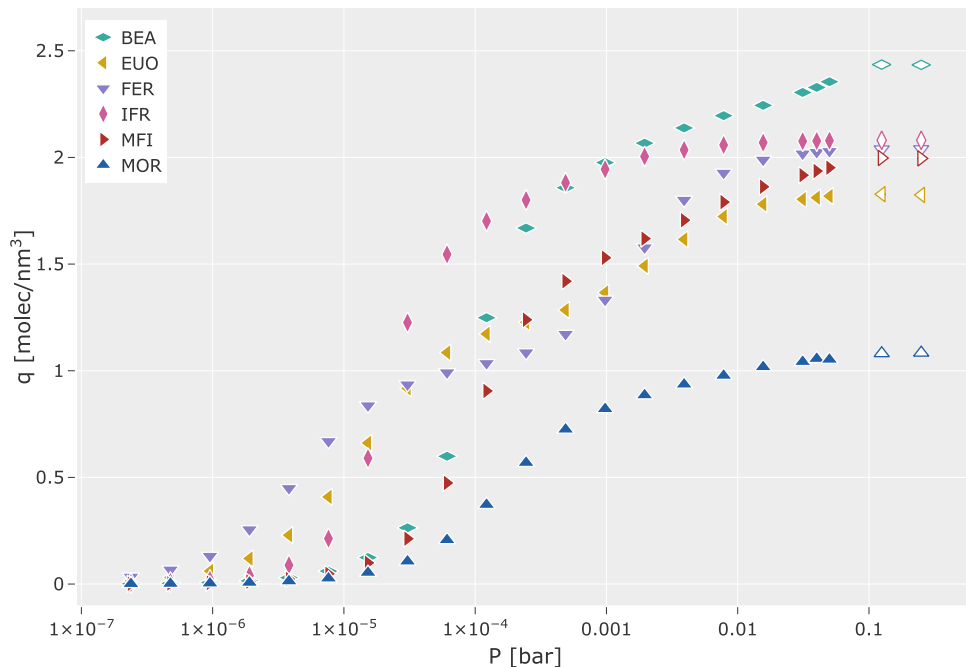


**Figure 4.** Predicted unary adsorption isotherms. The *y*-axis represents loadings (*q*) for six zeolite frameworks with pressure in the *x*-axis (logarithmic scale). Open symbols indicate adsorption from a liquid phase. Simulation uncertainties are smaller than symbol size.

## RESULTS AND DISCUSSION

**Force Field Validation for 1,4-Dioxane.** Before running adsorption simulations with 1,4-dioxane, we validated the force fields against simulation<sup>53</sup> and experimental data<sup>75</sup> from the literature (Figure 3a,b). To estimate the statistical uncertainties in the coexistence properties, 16 independent simulations were performed for temperatures ranging from 310 to 565 K with 80 000 MC cycles for equilibration and 100 000 MC cycles for production. The total volume of the two simulation boxes was adjusted so that the vapor phase contained roughly 50 molecules or about 10% of the total system size of 500 molecules. Our findings closely resemble simulated data in the literature and reasonably agree with experimental data. The critical temperature is overestimated by approximately 0.7%, and the normal boiling temperature is underestimated by 3.5%. The underestimation of normal boiling temperature is systematic in TraPPE-UA models<sup>76</sup> as they also tend to predict higher saturated vapor densities and pressures.

**Unary Adsorption Loadings for 1,4-Dioxane.** Single-component adsorption was studied at 300 K for 1,4-dioxane for a range of pressures, with the upper limit for vapor phase adsorption set to 0.05 bar so as not to exceed the saturation pressure ( $p_{\text{vap}}$ ) of 1,4-dioxane at 300 K, which is measured from simulations to be 0.105<sub>3</sub> bar. Two state points beyond  $p_{\text{vap}}$  were used to model adsorption from the liquid phase. The fluid box was initialized as a low-density gas at low pressures ( $p < p_{\text{vap}}$ ), or as a high-density liquid at higher pressures ( $p > p_{\text{vap}}$ ) to prevent nucleation issues. Eight independent simulations were performed for each framework with at least 80,000 equilibrations and 100,000 production cycles. Some of the frameworks required more time to reach equilibration, especially for higher pressure state points, but no simulation exceeded 500,000 MC cycles. We used the automated equilibrium detection technique described by Chodera<sup>77</sup> to determine which portion of the simulation runs from production cycles to use for reporting results. The technique determines an optimal amount of initial

data to be discarded as equilibration while minimizing the initial bias and variance. The pure 1,4-dioxane adsorption isotherms for the six zeolite frameworks are plotted in Figure 4.

Loading capacities for 1,4-dioxane at higher pressure follow the trend: BEA > IFR > FER > MFI > EUO > MOR. Frameworks with high-loading capacities like BEA or IFR may seem to be an optimal choice for an adsorbent, as literature studies with other adsorbent materials have reported that capacity is a limiting factor.<sup>26–28</sup>

However, our focus here is on modeling the adsorption behavior under environmental conditions, where 1,4-dioxane is found in low concentrations. Lower pressures correspond to low chemical potentials and low concentrations, and we observe upon closer inspection (Figure 5) that FER performs significantly better than the others in these low-pressure regions, with FER > EUO > IFR > BEA > MFI > MOR.

At lower pressures, adsorption is driven by the affinity between the adsorbate and the adsorbent. For all-Si zeolites, this is due to physisorption interactions in the pores and governed by pore size and shape.

Trends in the heats of adsorption and entropy of adsorption follow loading trends for the lowest state point ( $2.4 \times 10^{-7}$  bar), with MFI being the exception. The thermodynamic properties in Table 1 indicate that MFI pores have a looser fit than FER or EUO but a tighter fit when compared with IFR, which exhibits a higher loading capacity.

In simulations, there are two ways to calculate the average property of a thermodynamic system - ensemble average ( $\langle \frac{A}{B} \rangle$ ) and instantaneous average ( $\langle \frac{A}{B} \rangle$ ). Both approaches can result in different values. For some average calculations, it is problematic if *B* is sometimes zero, as  $\langle \frac{A}{B} \rangle$  is an average of terms that sometimes divide by zero. In our case, we calculated instantaneous measures of free energy of transfer (*dG*) for each frame, so our number is using  $\langle \frac{\rho_{\text{zeo}}}{\rho_{\text{fluid}}} \rangle$ . By defining *dG* to have

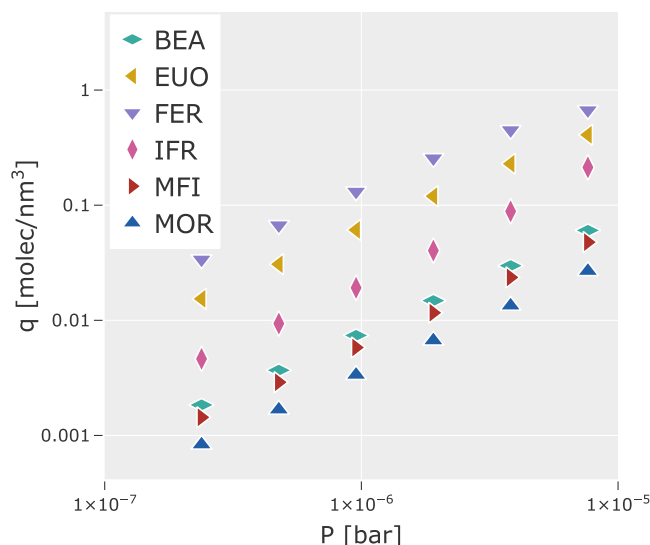


**Figure 5.** Inset view of Figure 4. Here, both loading and pressure are plotted on a logarithmic scale to clearly visualize the data points.

**Table 1. Thermodynamic Properties at the Lowest Pressure**

framework	heat of adsorption $\Delta H$ [kJ/mol]	free energy of transfer $\Delta G_{\text{fluid} \rightarrow \text{zeolite}}$ [kJ/mol]	entropy of adsorption $\Delta S$ [kJ/mol]
FER	-68.15 <sub>3</sub>	-38.87 <sub>4</sub>	-29.28 <sub>7</sub>
EUO	-57.70 <sub>1</sub>	-37.06 <sub>1</sub>	-20.64 <sub>2</sub>
IFR	-50.13 <sub>2</sub>	-33.97 <sub>1</sub>	-16.16 <sub>3</sub>
BEA	-47.60 <sub>2</sub>	-31.62 <sub>1</sub>	-15.98 <sub>3</sub>
MFI	-52.59 <sub>6</sub>	-31.00 <sub>3</sub>	-21.59 <sub>9</sub>
MOR	-45.70 <sub>3</sub>	-29.64 <sub>2</sub>	-16.06 <sub>5</sub>

$\rho_{\text{zeo}}$  in the numerator (and, since  $\rho_{\text{fluid}}$  is never zero), we avoid division by zero. However, when  $N_{\text{zeo}} = 0$ , we cannot compute enthalpy ( $\Delta H$ ) using  $\langle \frac{H_{\text{fluid}}}{N_{\text{fluid}}} \rangle - \langle \frac{H_{\text{zeo}}}{N_{\text{zeo}}} \rangle$ . Therefore, we removed the data points in which  $N_{\text{zeo}} = 0$  and still obtained the correct enthalpies of transfer.

Simulation snapshots show that 1,4-dioxane preferentially adsorbs into the smaller 8-membered ring of the FER framework at low pressures, as shown in Figure 6. The 8-ring pore of FER and 1,4-dioxane form a snug fit, which is a crucial factor for

selectivity in the adsorption of mixtures. An investigation on the adsorption of 1-butanol and water across distinct pore channels demonstrated how water coadsorption is specifically related to pore size.<sup>78</sup> Various other adsorption separation systems, including xylene isomers in MFI<sup>79</sup> and ethane/ethylene separations,<sup>80</sup> also show that when pore size and adsorbate molecules exhibit close conformity, the scope for coadsorption is considerably restricted. However, as the MC simulation trajectories are generated stochastically and include swap moves that directly insert molecules into the pores, these simulations cannot verify whether 1,4-dioxane molecules can diffuse through the surface to reach the smaller 8-ring pores of FER.

Chen and co-workers<sup>28</sup> demonstrated, using FTIR spectra and molecular dynamics simulation, that 1,4-dioxane fits tightly into the hydrophobic straight channels of TS-1 with a diameter of 5.6 Å. They also estimate the approximate size of the 1,4-dioxane molecule (5.2 × 5.9 × 6.7 Å) through van der Waal's projection and indicate that even though pore diameters are slightly smaller, the flexibility of either the adsorbate molecules or the zeolite structure promotes adsorption into zeolite channels.

**Mixture Adsorption at Environmental Concentrations.** We conducted a small test ( $NpT$ -Gibbs simulation with 120 1,4-dioxane and 600 water molecules at 1 atm and 300 K) to determine whether all-silica zeolites efficiently separate 1,4-dioxane from water under environmentally relevant conditions. While the test results were promising (we observed selective adsorption of 1,4-dioxane, with just about 14 molecules remaining in the liquid phase), we quickly realized that our simulation conditions were far from the parts-per-billion concentrations needed to model environmental conditions. Replicating the concentration of 1,4-dioxane that is considered safe for human health, i.e., 0.35 ppb (micrograms per liter of water) would require approximately 100 million water molecules for every molecule of 1,4-dioxane. Sampling with a regular  $NpT$ -Gibbs ensemble for such a system is not only impractical but also computationally inefficient; therefore, we developed an approach using gauge cells and extrapolation.

**Gauge Cells and Thermodynamic Extrapolation.** We performed simulations with 30 1,4-dioxane and 1800 water molecules, and we obtained different fluid concentrations by varying the 1,4-dioxane gauge cell volumes from  $100^3$  to  $310^3$  Å<sup>3</sup>.

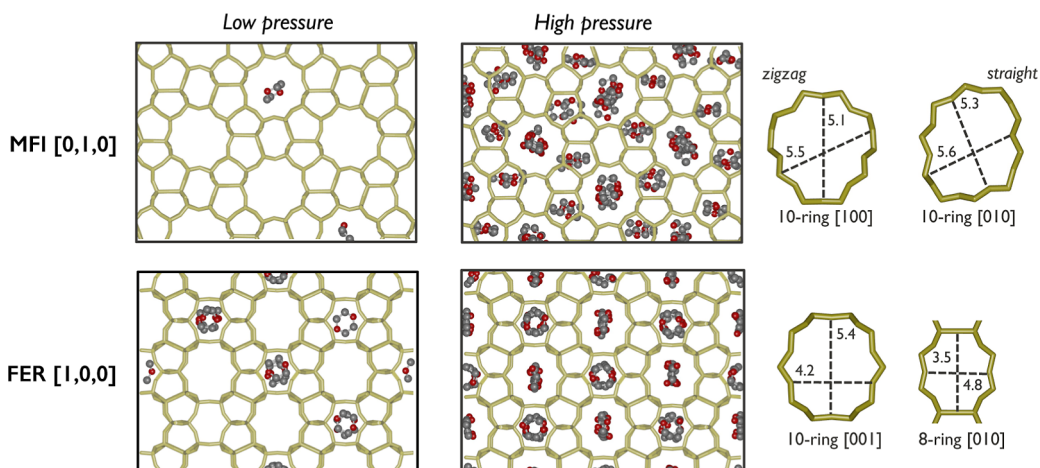


**Figure 6.** Loading of 1,4-dioxane at pore sites. Snapshots illustrating the loading of 1,4-dioxane in MFI (top row) and FER (bottom row) frameworks at low and high pressures.

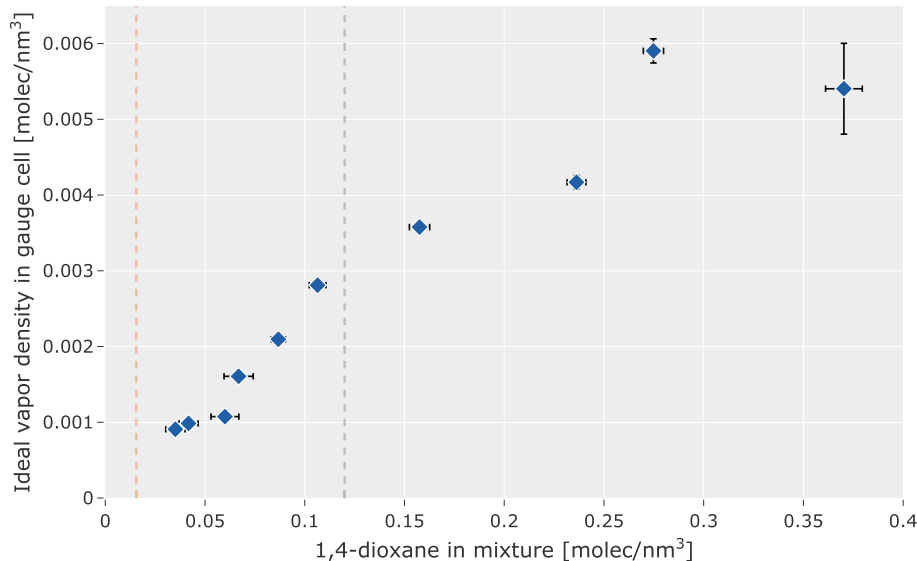


**Figure 7.** 1,4 dioxane concentration in the gauge cell versus in the liquid simulation box. The six lowest data points, to the left of the black dashed line, were used to calculate the change in Gibbs free energy ( $\Delta G$ ). The red dashed line represents the point where the liquid simulation box contains only one 1,4-dioxane molecule.

When we increased the simulation box side length beyond 310 Å, all 1,4-dioxane left the liquid simulation box; therefore, no statistically meaningful concentration remained. We set the water gauge cell size to maintain approximately 4 water molecules in the gauge cell. We then fixed this size ( $160^3 \text{ \AA}^3$ ) for all the state points analyzed, only changing the 1,4-dioxane gauge cell. Since the system under investigation is at a low temperature (300 K), we faced sampling challenges in particle insertions. Using rigid swaps for 1,4-dioxane, we had swap acceptance rates of about 0.001, even while considering 32 trials for insertion and 16 orientational trial positions. A drawback of using this gauge cell approach over traditional  $NpT$ -Gibbs is that we also cannot implement identity switch moves to boost sampling efficiency.

For each state point, eight independent simulations were conducted with a minimum of 400,000 MC cycles, and some state points required up to 500,000 cycles to equilibrate. While separate production runs were not performed for this setup, we used Chodera's equilibration detection method<sup>77</sup> to determine the regime of the data deemed to represent equilibrium. We determined the mean free energy of transfer for 1,4-dioxane at the six lowest concentrations in the liquid cell, as shown by the data points to the left of the black dashed line in Figure 7 and Table 2. Using that free energy and health-based reference concentration in eq 1, we computed the 1,4-dioxane

concentration in the gauge cell. Applying Henry's law for this concentration, we obtained a corresponding pressure of  $5.8 \times 10^{-11}$  bar for 1,4-dioxane. Figure S2 in Supporting Information includes the plot of pressure versus concentration, along with stepwise calculations for extrapolation. The pressure in the gauge cell of water is the average across the state points and is  $4.5 \times 10^{-2}$  bar. We finally used these pressures for 1,4-dioxane and water to set up  $NpT$ -Gibbs simulations at 300 K and model adsorption with 50 1,4-dioxane molecules and up to 1600 water molecules.

We used a series of gauge cell simulations to validate that the system is in the infinite dilution regime. A more efficient approach would be to perform gauge cell simulations at just one concentration (as low as possible) and obtain free energy of transfer ( $\Delta G$ ) from this. By using a series of simulations, however, we established that this system is in the Henry's law (infinite dilution) regime. While we do not have <1 molecule/simulation box, the linear trend suggests 1,4-dioxane–1,4-dioxane interactions are not significant.

When we impose the extrapolated 1,4-dioxane partial pressure and the water partial pressure on the zeolite box, our state point will be at a slightly lower total pressure than the 1 atm that was fixed thermodynamically in the gauge cell simulations due to the loss of some 1,4-dioxane. This should be a minor effect, given the extremely low concentrations. Alternatively, the water partial pressure for the extrapolated system could be obtained from a system of pure water; this assumes that the chemical potential of water with a parts-per-billion concentration of pollutant is nearer to pure water than it is to the water in our gauge cell simulations (which have a few 1,4-dioxane molecules).

**Selectivity in Mixture Adsorptions.** Mixture adsorption simulations were conducted across all zeolite frameworks by using four different zeolite box sizes. The baseline size was the minimal simulation cell (with at least 28 Å in  $x$ ,  $y$ , and  $z$ ), and box volumes were increased by factors of 2<sup>3</sup> to create supercells, as shown in Figure 2. The computational cost was managed by maintaining a rigid zeolite framework and using tabulated potentials to describe the zeolite/adsorbate interactions.<sup>74</sup> This approach enabled us to effectively sample the adsorption of 1,4-

**Table 2. Free Energy of Transfer for the Lowest Six State Points<sup>a</sup>**

$N_{14DX}^{mix}$	$\rho_{14DX}^{mix}$ [molec/nm <sup>3</sup> ]	$\Delta G_{14DX}^{*0}$ [kJ/mol]
2.3 <sub>3</sub>	0.035 <sub>5</sub>	-8.8 <sub>5</sub>
2.7 <sub>3</sub>	0.042 <sub>5</sub>	-9.3 <sub>3</sub>
3.8 <sub>4</sub>	0.060 <sub>7</sub>	-9.8 <sub>4</sub>
4.3 <sub>5</sub>	0.067 <sub>7</sub>	-9.2 <sub>3</sub>
5.6 <sub>2</sub>	0.087 <sub>4</sub>	-9.0 <sub>6</sub>
6.8 <sub>3</sub>	0.106 <sub>4</sub>	-8.8 <sub>5</sub>

<sup>a</sup>The average free energy is  $\overline{\Delta G_{14DX}^{*0}} = -9.2$  kJ/mol. The subscripts report uncertainty to the last significant figures of the mean values.

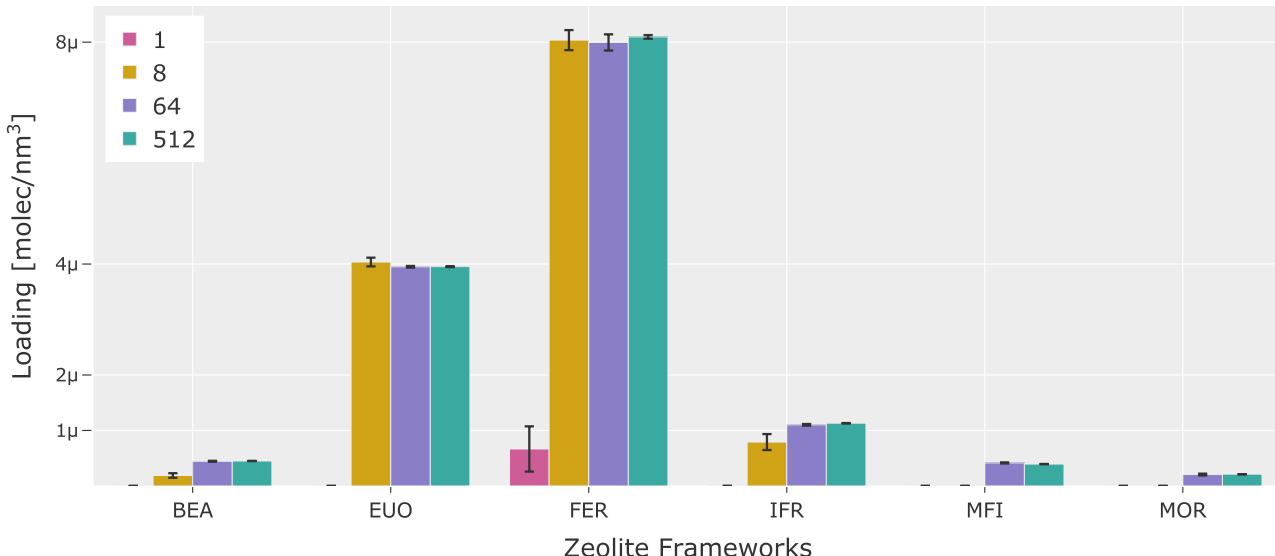


**Figure 8.** Predicted 1,4-dioxane loading from a 0.35 ppb aqueous solution. The *x*-axis lists the six zeolite frameworks for the four simulation box sizes (1, 8, 64, and 512 times the volume of the minimal simulation box for each framework) with loading in the *y*-axis.

dioxane at parts-per-billion concentrations in water, using up to 8192 zeolite unit cells in order to achieve reasonable statistics at low loading.

Eight independent simulations were conducted for each zeolite framework setup, with 180 000 equilibrations and 120 000 production cycles. Figure 8 illustrates the loading per unit volume of zeolites across different unit cell sizes. FER exhibits the best performance among all the zeolites, followed by EUO, IFR, BEA, MFI, and MOR. Notably, the smallest simulation box (the minimal size that accommodates a 14 Å cutoff, typical of MC simulations in zeolites, i.e., 2 × 4 × 2 unit cells for FER) and even the simulation box with 8× that volume were inadequate for collecting reasonable statistics. Simulations with 64× the minimal cell volume were sufficient to achieve accurate results for all zeolites; 512× did not demonstrate improvement and was thus not needed.

The mixture adsorption loadings follow the unary loadings trend when we extrapolate the 1,4-dioxane loadings in the unary simulations using Henry's Law down to the set pressure of 5.8 × 10<sup>-11</sup> bar for mixture adsorption loadings (Table 3). While

them rejects water and the other does not. They will have equal selectivities based on number density but different selectivities based on number ratio (because of different amounts of water rejection). Either may be relevant, depending on the application considerations.

$$\text{Selectivity, } S_{\text{ads,vol}} = \frac{\left(\frac{N_{\text{14DX}}}{\text{Volume}}\right)_{\text{zeolite}}}{R_c} \quad (4)$$

$$\text{Selectivity, } S_{\text{ads}} = \frac{\left(\frac{N_{\text{14DX}}}{N_{\text{water}}}\right)_{\text{zeolite}}}{R_c} \quad (5)$$

The simulations with large zeolite supercells are feasible only because of the excellent hydrophobicity of these materials; if much water were to coadsorb, the simulation would require more water molecules and become computationally expensive.

Table 4 summarizes the selectivity using a number ratio (eq 5) for 1,4-dioxane for each zeolite framework investigated. Selectivity is here defined as the ratio of 1,4-dioxane to water in the zeolite simulation box (eq 5), normalized by the health-based reference concentration of 1,4-dioxane in the number ratio, that is

**Table 4. Selectivity of the Frameworks at 1<sup>3</sup> (1), 2<sup>3</sup> (8), 4<sup>3</sup> (64), and 8<sup>3</sup> (512) Times the Minimal Simulation Cell<sup>a</sup>**

frameworks	S <sub>ads</sub> @1 (×106)	S <sub>ads</sub> @8 (×106)	S <sub>ads</sub> @64 (×106)	S <sub>ads</sub> @512 (×106)
BEA	0	0.33 <sub>8</sub>	0.78 <sub>2</sub>	0.81 <sub>1</sub>
EUO	0	2.01 <sub>4</sub>	1.98 <sub>2</sub>	1.97 <sub>1</sub>
IFR	0	0.82 <sub>2</sub>	0.12 <sub>3</sub>	0.11 <sub>1</sub>
FER	0.75 <sub>5</sub>	8.76 <sub>2</sub>	8.70 <sub>2</sub>	8.72 <sub>4</sub>
MFI	0	0	0.24 <sub>1</sub>	0.23 <sub>1</sub>
MOR	0	0	0.11 <sub>1</sub>	0.11 <sub>1</sub>

**Table 3. 1,4-Dioxane Loadings Are Similar in Unary and Mixture Systems at Extrapolated Pressure**

framework	loading @unary [molec/nm <sup>3</sup> ]	loading @512 [molec/nm <sup>3</sup> ]
FER	5.6 × 10 <sup>-6</sup>	8.1 × 10 <sup>-6</sup>
EUO	3.2 × 10 <sup>-6</sup>	3.9 × 10 <sup>-6</sup>
IFR	1.5 × 10 <sup>-6</sup>	1.1 × 10 <sup>-6</sup>
BEA	4.6 × 10 <sup>-7</sup>	4.5 × 10 <sup>-7</sup>
MFI	3.6 × 10 <sup>-7</sup>	4.1 × 10 <sup>-7</sup>
MOR	2.0 × 10 <sup>-7</sup>	2.1 × 10 <sup>-7</sup>

unary adsorption trends alone could potentially identify the best framework for adsorption, our method provides accurate estimates of the selectivity and loadings under specific environmental conditions.

We define and consider two selectivity measures: one based on number density (eq 4) and the other based on number ratio (eq 5). Hypothetically, consider two zeolites, each of which increases the number density of 1,4-dioxane by a factor of 10<sup>6</sup> between the aqueous phase and the zeolite phase, but one of

<sup>a</sup>All values were calculated from each of the eight independent simulations and reported as the mean, and uncertainties are reported in subscripts as the standard error of the mean to last significant figures. S<sub>ads</sub> = 0 indicates that negligible 1,4-dioxane was adsorbed in the zeolite.

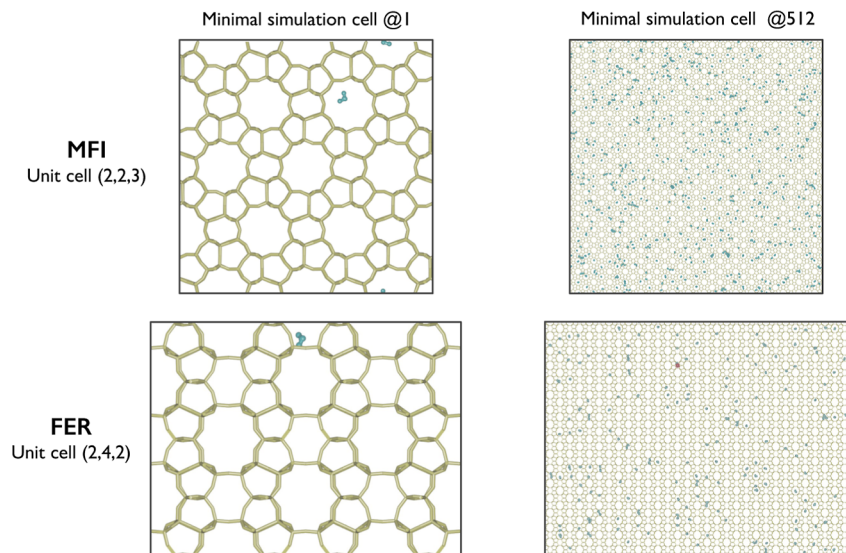


**Figure 9.** Simulation snapshots from mixture adsorptions show that FER rejects more water than MFI. The water ratio in MFI to FER is 3.8 across the unit cell volumes; blue represents water molecules, which are denser in MFI unit cells, and red represents 1,4-dioxane, which was only observed in a simulation frame for the FER framework.

$$R_c = 0.35 \text{ ppb} = 0.35 \mu\text{g/L} = \frac{N_{14\text{DX}}}{N_{\text{water}}} = 7.17 \times 10^{-11} \quad (6)$$

All zeolites are extremely selective, with enrichment in the zeolite phase relative to the water phase by at least a factor of  $1 \times 10^5$ . FER is even more selective, with  $S_{\text{ads}}$  of  $8.7 \times 10^6$ . The volume-based selectivity (eq 4) is calculated by replacing the number of water molecules in the zeolite with its framework volume in eq 5. These results are displayed in Table S4 in the Supporting Information and illustrate that these volume-based selectivities are also high with the same trends. Additionally, Figure 9 showcases snapshots of the mixture adsorption loadings in FER, varying across different unit cell sizes. The selectivity trends at 512× are similar to unary 1,4-dioxane loadings (Table 3), with FER > EUO > BEA > MFI > IFR  $\approx$  MOR. However, these do not exactly match the trends in unary adsorption because of different levels of water rejection. IFR dropping two ranks indicates it relatively rejects less water than MFI and BEA. Trends in selectivity with simulation box volume also indicate that 8× or 64× the minimal cell were needed to accurately measure these.

Despite being extremely selective adsorbents, these zeolites are nearly devoid of 1,4-dioxane; in even the most selective framework, FER, <1 molecules are present among 8196 unit cells (Table S5). This is *not* related to the selectivity/capacity trade-offs often discussed in gas adsorption;<sup>81–83</sup> Figures 4 and 6 show each can accommodate >1 molecules/unit cell. Instead, this is an intrinsic characteristic (and challenge) for adsorbing mixtures with ppb concentrations. After all, increasing the ppb concentration by  $10^6$  still leaves a low concentration of 0.1%. Only when the adsorbent starts getting saturated will capacity start playing a role; such may occur for materials with even higher selectivities than those described here, or for materials in which adsorption is dominated by a few active sites.

From the number of 1,4-dioxane and water molecules adsorbed in the zeolite framework (Tables S5 and S6), we can perform mass balance calculations to determine its efficacy in filtering 1 L of water to produce a 0.35 ppb outlet stream. For example, 1 g of FER removes 65% of 1,4-dioxane from a feed

with a concentration of 0.99 ppb, while the same amount of MOR removes only 5% from a feed with a concentration of 0.37 ppb. Table S7 in Supporting Information lists some predicted amounts of removal using 1, 10, and 100 g of zeolite for both FER and MOR frameworks.

## CONCLUSIONS AND OUTLOOK

Accurately modeling water treatment systems is challenging due to the presence of numerous unknown substances, which vary in their concentrations and often interact with each other. This study addresses two key challenges: identifying effective adsorbents for an emerging water pollutant and sampling the system under environmentally relevant concentrations. This methodology sets the stage for further exploration of effective adsorbents for other emerging contaminants, such as PFAS, arsenic, and chlorinated species. However, our computational methodology is contingent upon both the adsorbent's selectivity for the target pollutant and its ability to reject solvent simultaneously. This limits the approach's applicability to certain adsorption systems (e.g., very hydrophobic sorbents).

These simulations identify FER as a promising material for 1,4-dioxane separation from water. The unary adsorption simulations showed that the 8-membered ring pores in FER snugly accommodate 1,4 dioxane. Furthermore, our mixture adsorption simulations with water indicate that FER possesses exceptional selectivity for low concentrations of 1,4-dioxane; it particularly becomes more apparent in simulations with the supercell construction of zeolite frameworks. However, MC simulations do account for diffusion, which may impose transport barriers for 1,4-dioxane. Nonetheless, we think that all-Si FER and all-Si EUO are promising materials for further investigation.

The adsorbed concentration differs significantly from the environmental concentrations, implying that hydrophobic all-silica zeolites are ultraselective adsorbents, as the latter can be considered to be infinitely diluted. However, it is challenging to synthesize them without defects,<sup>19</sup> which enable water coadsorption and would undermine selectivity. This work aims to motivate the synthesis of these zeolites to be used in

various separation processes, particularly in water pollutant remediation, where these interactions can play a crucial role. We also achieve large selectivities here while only involving physisorption interactions because of the tight fit of 1,4-dioxane in FER. In other contexts, chemisorption is used to remove trace contaminants from water<sup>84–86</sup> as the means of providing a strong intrinsic interaction to pull the dilute solute from the solution. Traditional MC simulations do not have interaction potentials or efficient sampling techniques for chemisorption; the development of these could further extend the applicability of this approach.

## ■ ASSOCIATED CONTENT

### ① Supporting Information

The Supporting Information is available free of charge at <https://pubs.acs.org/doi/10.1021/acs.jctc.4c00236>.

Simulation source code (version of MCCCS-MN software used in this work), along with sample input files for all the setups (VLCC, gcMC, and NPT-Gibbs) and their output files for one independent simulation, are available at [https://github.com/ATOMSLab/14DX\\_Ad-sorption](https://github.com/ATOMSLab/14DX_Ad-sorption) (ZIP)

Information on the zeolite frameworks and all the force field parameters, derivation of the expression for the free energy of transfer, detailed working steps of the thermodynamic extrapolation approach, and additional tables for analyzing selectivity across the zeolite frameworks ([PDF](#))

## ■ AUTHOR INFORMATION

### Corresponding Author

**Tyler R. Josephson** — Department of Chemical, Biochemical, and Environmental Engineering, University of Maryland Baltimore County, Baltimore, Maryland 21250, United States; Department of Computer Science and Electrical Engineering, University of Maryland Baltimore County, Baltimore, Maryland 21250, United States;  [orcid.org/0000-0002-0100-0227](https://orcid.org/0000-0002-0100-0227); Email: [tjo@umbc.edu](mailto:tjo@umbc.edu)

### Authors

**Samiha Sharlin** — Department of Chemical, Biochemical, and Environmental Engineering, University of Maryland Baltimore County, Baltimore, Maryland 21250, United States

**Rodrigo A. Lozano** — Department of Chemistry, University of California Irvine, Irvine, California 92617, United States

Complete contact information is available at:

<https://pubs.acs.org/10.1021/acs.jctc.4c00236>

### Notes

The authors declare no competing financial interest.

## ■ ACKNOWLEDGMENTS

This material is based upon work supported by the National Science Foundation under Grant #2138938, as well as startup funds from the University of Maryland, Baltimore County.

## ■ REFERENCES

- (1) Deischter, J.; Müller, F.; Bong, B.; Maurer, C.; Hartmann, S. S.; Palkovits, R. Separation by Size Exclusion: Selective Liquid-Phase Adsorption of L-Lysine from Lysine–Glucose Mixtures on Zeolites. *ACS Sustainable Chem. Eng.* **2022**, *10*, 10211–10222.
- (2) Dauenhauer, P. J.; Abdelrahman, O. A. A universal descriptor for the entropy of adsorbed molecules in confined spaces. *ACS Cent. Sci.* **2018**, *4*, 1235–1243.
- (3) Kumar, S.; Srivastava, R.; Koh, J. Utilization of zeolites as CO<sub>2</sub> capturing agents: Advances and future perspectives. *J. CO<sub>2</sub> Util.* **2020**, *41*, 101251.
- (4) Xu, J.; Xu, Y.; Bu, X.-H. Advances in Emerging Crystalline Porous Materials. *Small* **2021**, *17* (22), No. e2102331.
- (5) Corma, A. State of the art and future challenges of zeolites as catalysts. *J. Catal.* **2003**, *216*, 298–312.
- (6) Keil, F. J.; Krishna, R.; Coppens, M.-O. Modeling of diffusion in zeolites. *Rev. Chem. Eng.* **2000**, *16*, 71–197.
- (7) Townsend, R. P.; Coker, E. N. Chapter 11 Ion Exchange in Zeolites; Elsevier, 2001; Vol. 137, pp 467–524.
- (8) Margeta, K.; Farkaš, A. Introductory chapter: zeolites—from discovery to new applications on the global market. In *Zeolites—New Challenges*; Margeta, K.; Farkaš, A., Ed., 2020, pp 1–10.
- (9) Kumar, L.; Kaur, R.; Sharma, J. The efficiency of zeolites in water treatment for combating ammonia—An experimental study on Yamuna River water & treated sewage effluents. *Inorg. Chem. Commun.* **2021**, *134*, 108978.
- (10) Bolisetty, S.; Peydayesh, M.; Mezzenga, R. Sustainable technologies for water purification from heavy metals: review and analysis. *Chem. Soc. Rev.* **2019**, *48*, 463–487.
- (11) Jiménez-Reyes, M.; Almazán-Sánchez, P.; Solache-Ríos, M. Radioactive waste treatments by using zeolites. A short review. *J. Environ. Radioact.* **2021**, *233*, 106610.
- (12) Roshanfekr Rad, L.; Anbia, M. Zeolite-based composites for the adsorption of toxic matters from water: A review. *J. Environ. Chem. Eng.* **2021**, *9*, 106088.
- (13) Jiang, N.; Shang, R.; Heijman, S. G.; Rietveld, L. C. High-silica zeolites for adsorption of organic micro-pollutants in water treatment: A review. *Water Res.* **2018**, *144*, 145–161.
- (14) Cinar, S.; Beler-Baykal, B. Ion exchange with natural zeolites: an alternative for water softening? *Water Sci. Technol.* **2005**, *51*, 71–77.
- (15) Swenson, P.; Tanchuk, B.; Gupta, A.; An, W.; Kuznicki, S. M. Pervaporative desalination of water using natural zeolite membranes. *Desalination* **2012**, *285*, 68–72.
- (16) Smit, B.; Maesen, T. L. Molecular simulations of zeolites: adsorption, diffusion, and shape selectivity. *Chem. Rev.* **2008**, *108*, 4125–4184.
- (17) Baerlocher, C.; McCusker, L. *Database of Zeolite Structures*. <http://www.iza-structure.org/databases/> (accessed June 21, 2024).
- (18) Cundy, C. S.; Cox, P. A. The hydrothermal synthesis of zeolites: Precursors, intermediates and reaction mechanism. *Microporous Mesoporous Mater.* **2005**, *82*, 1–78.
- (19) Burton, A. W.; Zones, S. I.; Elomari, S. The chemistry of phase selectivity in the synthesis of high-silica zeolites. *Curr. Opin. Colloid Interface Sci.* **2005**, *10*, 211–219.
- (20) Anderson, M. A. Removal of MTBE and other organic contaminants from water by sorption to high silica zeolites. *Environ. Sci. Technol.* **2000**, *34*, 725–727.
- (21) Pollitt, K. J. G.; Kim, J.-H.; Peccia, J.; Elimelech, M.; Zhang, Y.; Charkoftaki, G.; Hodges, B.; Zucker, I.; Huang, H.; Deziel, N. C.; et al. 1, 4-Dioxane as an emerging water contaminant: State of the science and evaluation of research needs. *Sci. Total Environ.* **2019**, *690*, 853–866.
- (22) Adamson, D. T.; Piña, E. A.; Cartwright, A. E.; Rauch, S. R.; Hunter Anderson, R.; Mohr, T.; Connor, J. A. 1, 4-Dioxane drinking water occurrence data from the third unregulated contaminant monitoring rule. *Sci. Total Environ.* **2017**, *596*, 596–597, 236–245.
- (23) Mohr, T. K.; DiGuiseppi, W. H.; Hatton, J. W.; Anderson, J. K. *Environmental Investigation and Remediation: 1, 4-dioxane and Other Solvent Stabilizers*; CRC Press, 2020.
- (24) McElroy, A. C.; Hyman, M. R.; Knappe, D. R. 1, 4-Dioxane in drinking water: emerging for 40 years and still unregulated. *Curr. Opin. Environ. Sci. Health.* **2019**, *7*, 117–125.

- (25) Chiang, S.-Y.; Anderson, R.; Wilken, M.; Walecka-Hutchison, C. Practical perspectives of 1, 4-dioxane investigation and remediation. *Remediation J.* **2016**, *27*, 7–27.
- (26) Woodard, S.; Mohr, T.; Nickelsen, M. G. Synthetic media: A promising new treatment technology for 1, 4-dioxane. *Remediation J.* **2014**, *24*, 27–40.
- (27) Fukuhara, T.; Iwasaki, S.; Hasegawa, T.; Ishihara, K.; Fujiwara, M.; Abe, I. Adsorption of 1, 4-dioxane from aqueous solutions onto various activated carbons. *J. Water Environ. Nanotechnol.* **2011**, *9*, 249–258.
- (28) Chen, R.; Liu, C.; Johnson, N. W.; Zhang, L.; Mahendra, S.; Liu, Y.; Dong, Y.; Chen, M. Removal of 1,4-dioxane by titanium silicalite-1: Separation mechanisms and bioregeneration of sorption sites. *Chem. Eng. J.* **2019**, *371*, 193–202.
- (29) Sherman, J. D. Synthetic zeolites and other microporous oxide molecular sieves. *Proc. Natl. Acad. Sci. U.S.A.* **1999**, *96*, 3471–3478.
- (30) Wragg, D. S.; Morris, R. E.; Burton, A. W. Pure Silica Zeolite-type Frameworks: A Structural Analysis. *Chem. Mater.* **2008**, *20*, 1561–1570.
- (31) Smit, B.; Krishna, R. Molecular simulations in zeolitic process design. *Chem. Eng. Sci.* **2003**, *58*, 557–568.
- (32) Fuchs, A. H.; Cheetham, A. K. Adsorption of guest molecules in zeolitic materials: Computational aspects. *J. Phys. Chem. B* **2001**, *105*, 7375–7383.
- (33) Catlow, C. R. A.; Bell, R.; Gale, J.; Lewis, D. *Modelling of Structure and Reactivity in Zeolites*; Elsevier, 1995; Vol. 97, pp 87–100..
- (34) Catlow, C. R. A.; Smit, B.; van Santen, R. *Computer Modelling of Microporous Materials*; Elsevier, 2004.
- (35) Neimark, A. V.; Vishnyakov, A. Gauge cell method for simulation studies of phase transitions in confined systems. *Phys. Rev. E* **2000**, *62*, 4611–4622.
- (36) Vishnyakov, A.; Neimark, A. V. Studies of Liquid–Vapor equilibria, criticality, and spinodal transitions in nanopores by the gauge cell Monte Carlo simulation method. *J. Phys. Chem. B* **2001**, *105*, 7009–7020.
- (37) Neimark, A. V.; Vishnyakov, A. A simulation method for the calculation of chemical potentials in small, inhomogeneous, and dense systems. *J. Chem. Phys.* **2005**, *122*, 234108.
- (38) Clark, M. D.; Morris, K. R.; Tomassone, M. S. Correlation of solubility with the metastable limit of nucleation using gauge-cell monte carlo simulations. *Langmuir* **2017**, *33*, 9081–9090.
- (39) Gor, G. Y.; Rasmussen, C. J.; Neimark, A. V. Capillary condensation hysteresis in overlapping spherical pores: A Monte Carlo simulation study. *Langmuir* **2012**, *28*, 12100–12107.
- (40) Neimark, A. V.; Vishnyakov, A. Monte Carlo simulation study of droplet nucleation. *J. Chem. Phys.* **2005**, *122*, 174508.
- (41) Zheng, F.; Zhang, X.; Wang, W. Macrophase and microphase separations for surfactants adsorbed on solid surfaces: A gauge cell Monte Carlo study in the lattice model. *Langmuir* **2008**, *24*, 4661–4669.
- (42) Siderius, D. W.; Hatch, H. W.; Shen, V. K. Temperature Extrapolation of Henry's Law Constants and the Isosteric Heat of Adsorption. *J. Phys. Chem. B* **2022**, *126*, 7999–8009.
- (43) Mahynski, N. A.; Errington, J. R.; Shen, V. K. Multivariable extrapolation of grand canonical free energy landscapes. *J. Chem. Phys.* **2017**, *147*, 234111.
- (44) Cichowski, E. C.; Schmidt, T. R.; Errington, J. R. Determination of Henry's law constants through transition matrix Monte Carlo simulation. *Fluid Phase Equilif.* **2005**, *236*, 58–65.
- (45) Luo, J.; Farrell, J. Examination of hydrophobic contaminant adsorption in mineral micropores with grand canonical Monte Carlo simulations. *Environ. Sci. Technol.* **2003**, *37*, 1775–1782.
- (46) Siepmann, J.; Martin, M.; Chen, B.; Wick, C.; Stubbs, J.; Potoff, J.; Eggimann, B.; McGrath, M.; Zhao, X.; Anderson, K.; et al. *Monte Carlo for Complex Chemical Systems—Minnesota*, 2017.
- (47) Panagiotopoulos, A. Z. Direct determination of phase coexistence properties of fluids by Monte Carlo simulation in a new ensemble. *Mol. Phys.* **1987**, *61*, 813–826.
- (48) Smit, B. d.; De Smedt, P.; Frenkel, D. Computer simulations in the Gibbs ensemble. *Mol. Phys.* **1989**, *68*, 931–950.
- (49) Panagiotopoulos, A. Z.; Quirke, N.; Stapleton, M.; Tildesley, D. Phase equilibria by simulation in the Gibbs ensemble: alternative derivation, generalization and application to mixture and membrane equilibria. *Mol. Phys.* **1988**, *63*, 527–545.
- (50) Ben-Naim, A. Y. *Statistical Thermodynamics for Chemists and Biochemists*; Springer Science & Business Media: New York, 2013.
- (51) Martin, M. G.; Siepmann, J. I. Calculating Gibbs free energies of transfer from Gibbs ensemble Monte Carlo simulations. *Theor. Chem. Acc.* **1998**, *99*, 347–350.
- (52) Transferable Potentials for Phase Equilibria. <http://trappe.umn.edu/> (accessed June 21, 2024).
- (53) Keasler, S. J.; Charan, S. M.; Wick, C. D.; Economou, I. G.; Siepmann, J. I. Transferable potentials for phase equilibria—united atom description of five-and six-membered cyclic alkanes and ethers. *J. Phys. Chem. B* **2012**, *116*, 11234–11246.
- (54) Bai, P.; Tsapatsis, M.; Siepmann, J. I. TraPPE-zeo: Transferable potentials for phase equilibria force field for all-silica zeolites. *J. Phys. Chem. C* **2013**, *117*, 24375–24387.
- (55) Eggimann, B. L.; Sun, Y.; DeJaco, R. F.; Singh, R.; Ahsan, M.; Josephson, T. R.; Siepmann, J. I. Assessing the quality of molecular simulations for vapor–liquid equilibria: An analysis of the TraPPE database. *J. Chem. Eng. Data* **2020**, *65*, 1330–1344.
- (56) Jorgensen, W. L.; Chandrasekhar, J.; Madura, J. D.; Impey, R. W.; Klein, M. L. Comparison of simple potential functions for simulating liquid water. *J. Chem. Phys.* **1983**, *79*, 926–935.
- (57) Chen, B.; Siepmann, J. I. Microscopic structure and solvation in dry and wet octanol. *J. Phys. Chem. B* **2006**, *110*, 3555–3563.
- (58) Rafferty, J. L.; Siepmann, J. I.; Schure, M. R. Molecular-level comparison of alkylsilane and polar-embedded reversed-phase liquid chromatography systems. *Anal. Chem.* **2008**, *80*, 6214–6221.
- (59) Rafferty, J. L.; Sun, L.; Siepmann, J. I.; Schure, M. R. Investigation of the driving forces for retention in reversed-phase liquid chromatography: Monte Carlo simulations of solute partitioning between n-hexadecane and various aqueous–organic mixtures. *Fluid Phase Equilib.* **2010**, *290*, 25–35.
- (60) Shah, M. S.; Tsapatsis, M.; Siepmann, J. I. Monte Carlo simulations probing the adsorptive separation of hydrogen sulfide/methane mixtures using all-silica zeolites. *Langmuir* **2015**, *31*, 12268–12278.
- (61) Pahari, S.; Dorneles de Mello, M.; Shah, M. S.; Josephson, T. R.; Ren, L.; Nguyen, H. G. T.; Van Zee, R. D.; Tsapatsis, M.; Siepmann, J. I. Ethanol and Water Adsorption in Conventional and Hierarchical All-Silica MFI Zeolites. *ACS Phys. Chem. Au* **2022**, *2*, 79–88.
- (62) Dubbeldam, D.; Torres-Knoop, A.; Walton, K. S. On the inner workings of Monte Carlo codes. *Mol. Simul.* **2013**, *39*, 1253–1292.
- (63) Allen, M. P.; Tildesley, D. J. *Computer Simulation of Liquids*; Oxford University Press, 2017.
- (64) Metropolis, N.; Rosenbluth, A. W.; Rosenbluth, M. N.; Teller, A. H.; Teller, E. Equation of state calculations by fast computing machines. *J. Chem. Phys.* **1953**, *21*, 1087–1092.
- (65) Siepmann, J. I. A method for the direct calculation of chemical potentials for dense chain systems. *Mol. Phys.* **1990**, *70*, 1145–1158.
- (66) Siepmann, J. I.; Frenkel, D. Configurational bias Monte Carlo: a new sampling scheme for flexible chains. *Mol. Phys.* **1992**, *75*, 59–70.
- (67) Martin, M. G.; Siepmann, J. I. Novel configurational-bias Monte Carlo method for branched molecules. Transferable potentials for phase equilibria. 2. United-atom description of branched alkanes. *J. Phys. Chem. B* **1999**, *103*, 4508–4517.
- (68) Calero, S. Comprehensive Inorganic Chemistry II. In *From Elements to Applications*, 2nd ed.; Reedijk, J.; Poepelmeier, K., Ed.; Elsevier Ireland Ltd, 2013; pp 989–1006.
- (69) Vlugt, T.; Martin, M.; Smit, B.; Siepmann, J.; Krishna, R. Improving the efficiency of the configurational-bias Monte Carlo algorithm. *Mol. Phys.* **1998**, *94*, 727–733.
- (70) Martin, M. G.; Thompson, A. P. Industrial property prediction using Towhee and LAMMPS. *Fluid Phase Equilif.* **2004**, *217*, 105–110.

- (71) Martin, M. G.; Biddy, M. J. Monte Carlo molecular simulation predictions for the heat of vaporization of acetone and butyramide. *Fluid Phase Equilib.* **2005**, *236*, 53–57.
- (72) Martin, M. G.; Frischknecht, A. L. Using arbitrary trial distributions to improve intramolecular sampling in configurational-bias Monte Carlo. *Mol. Phys.* **2006**, *104*, 2439–2456.
- (73) Wick, C. D.; Siepmann, J. I. Self-adapting fixed-end-point configurational-bias Monte Carlo method for the regrowth of interior segments of chain molecules with strong intramolecular interactions. *Macromolecules* **2000**, *33*, 7207–7218.
- (74) June, R. L.; Bell, A. T.; Theodorou, D. N. Prediction of low occupancy sorption of alkanes in silicalite. *J. Phys. Chem.* **1990**, *94*, 1508–1516.
- (75) Linstrom, P.; Mallard, W. G.; E. NIST Chemistry WebBook *NIST Standard Reference Database Number 69*; National Institute of Standards and Technology: Gaithersburg, MD, 2023..
- (76) Chen, B.; Siepmann, J. I. Transferable potentials for phase equilibria. 3. Explicit-hydrogen description of normal alkanes. *J. Phys. Chem. B* **1999**, *103*, 5370–5379.
- (77) Chodera, J. D. A simple method for automated equilibration detection in molecular simulations. *J. Chem. Theory Comput.* **2016**, *12*, 1799–1805.
- (78) DeJaco, R. F.; Bai, P.; Tsapatsis, M.; Siepmann, J. I. Adsorptive separation of 1-butanol from aqueous solutions using MFI- and FER-type zeolite frameworks: a Monte Carlo study. *Langmuir* **2016**, *32*, 2093–2101.
- (79) Yang, Y.; Bai, P.; Guo, X. Separation of xylene isomers: a review of recent advances in materials. *Ind. Eng. Chem. Res.* **2017**, *56*, 14725–14753.
- (80) Bereciartua, P. J.; Cantín, Á.; Corma, A.; Jordá, J. L.; Palomino, M.; Rey, F.; Valencia, S.; Corcoran, E. W., Jr; Kortunov, P.; Ravikovich, P. I.; et al. Control of zeolite framework flexibility and pore topology for separation of ethane and ethylene. *Science* **2017**, *358*, 1068–1071.
- (81) Kumar, N.; Mukherjee, S.; Harvey-Reid, N. C.; Bezrukov, A. A.; Tan, K.; Martins, V.; Vandichel, M.; Pham, T.; van Wyk, L. M.; Oyekan, K.; et al. Breaking the trade-off between selectivity and adsorption capacity for gas separation. *Chem.* **2021**, *7*, 3085–3098.
- (82) Garcia, E. J.; Perez-Pellitero, J.; Pirngruber, G. D.; Jallut, C.; Palomino, M.; Rey, F.; Valencia, S. Tuning the adsorption properties of zeolites as adsorbents for CO<sub>2</sub> separation: best compromise between the working capacity and selectivity. *Ind. Eng. Chem. Res.* **2014**, *53*, 9860–9874.
- (83) Yeo, B. C.; Kim, D.; Kim, H.; Han, S. S. High-throughput screening to investigate the relationship between the selectivity and working capacity of porous materials for propylene/propane adsorptive separation. *J. Phys. Chem. C* **2016**, *120*, 24224–24230.
- (84) Rajaković, L. V.; Mitrović, M. M. Arsenic removal from water by chemisorption filters. *Environ. Pollut.* **1992**, *75*, 279–287.
- (85) Renu, M. A.; Singh, K.; Upadhyaya, S.; Dohare, R. Removal of heavy metals from wastewater using modified agricultural adsorbents. *Mater. Today: Proc.* **2017**, *4*, 10534–10538.
- (86) Gagliano, E.; Sgroi, M.; Falciglia, P. P.; Vagliasindi, F. G.; Roccaro, P. Removal of poly-and perfluoroalkyl substances (PFAS) from water by adsorption: Role of PFAS chain length, effect of organic matter and challenges in adsorbent regeneration. *Water Res.* **2020**, *171*, 115381.